Impact of a Cu_2BaSnS_4 HTL on Interface Recombination Kinetics of Formamidinium Perovskite Solar Cells

Alok Singh Kushwaha[1], Arunesh Pratap Singh[1], Shailendra Kumar Mishra[1], Alok Agarwal[2]

[1]Department of Computer Science Engineering, Parul University, Vadodara, Gujarat, India, [2]Department of Electronics and Communication Engineering, Aravali College of Engineering and Management, Haryana, India
alok.kushwaha35214@paruluniversity.ac.in

Abstract. Formamidine exhibits favourable optoelectronic characteristics and significant potential and enhanced thermal stability as a perovskite; however, their device performance is often constrained by interfacial charge losses and defect-mediated recombination processes. In this work, comprehensive numerical simulations are carried out to systematically evaluate the influence of intrinsic material parameters and buffer layer engineering on the PSC characteristics. The interfacial defect, charge carrier mobility, energy band alignment and thickness of layers are rigorously optimized to minimize recombination losses and enhance charge transport. The results indicate that the introduction of an appropriately engineered buffer layer significantly improves interfacial issues and reduces charge recombination, which significantly increases power conversion efficiency. The findings offer valuable theoretical insights and practical design guidance for achieving high-performance and durable formamidinium-based perovskite solar cell architectures. To ensure the reliability of the model, the simulation parameters were calibrated using experimentally reported data

Keywords: Formamidinium perovskites; HTL; ETL; Band gap

1 Introduction

Extensive research is currently focused on solar energy, as it is promising , sustainable , green and alternative to conventional fossil fuels [1] . The development of solar cell technologies is generally described in terms of successive generations, beginning with crystalline silicon devices, followed by thin-film systems, and extending to emerging perovskite, organic, and hybrid nanostructured photovoltaic architectures [2]. The present work investigates the role of different electron and hole transport layers, together with various electrode configurations, in determining the photovoltaic characteristics of $FA_{1-x}Cs_xPb(I_{1-x}Br_x)_3$ based mixed-cation perovskite solar cells. $FAPbI_3$ is regarded as an efficient photovoltaic absorber due to its near-ideal bandgap and strong optoelectronic properties, while partial substitution with cesium in $FA_{1-x}Cs_xPbI_3$ significantly enhances phase stability and device durability [3]. Formamidinium lead iodide ($FAPbI_3$) exhibits Eg 1.48 eV, which is close to theoretically upper bound defined by

© The Author(s) 2026
J. Saxena et al. (eds.), *Proceedings of the International Conference on Sustainable Micro-Nano Materials & Innovative Technology (ICSUMMIT 2026)*, Atlantis Highlights in Engineering 44,
https://doi.org/10.2991/978-94-6239-727-9_24

the Shockley–Queisser for photovoltaic devices, thereby supporting its suitability for high-performance solar cell applications [4]. Cu_2BaSnS_4 exhibits a direct bandgap in the range of 1.3–1.9 eV [12,13]. Due to having favourable band alignment and good carrier mobility it is used as HTL [14,15], along with a high optical absorption coefficient ($>10^4$ cm^{-1}), making it highly suitable for thin-film solar cell applications [1], [2].

2 PSC Device Architecture and Material Selection

The planar heterojunction device structure, FTO/ETL/Formamidine/HTL(Cu_2BaSnS_4)/rear metal electrode (Au). Cu_2BaSnS_4 was selected as the p-type material, over absorber, for material stability, which together support efficient hole extraction and improved device performance [5]. One-dimensional numerical simulation tool, Capacitance Simulator developed by Gent University, is used to investigate the impact of different HTL, ETL, and electrode combinations for photovoltaic studies such as Voc, fill factor (FF), and PCE (%) [6]. The material properties presented in Table 1 were compiled from a comprehensive review of the existing literature. We first validate the model with the experimental results under similar conditions mentioned by S. Karthick et al. in their research paper. They obtained Jsc (mA/cm^2) of 16.6, FF (%) of 40.6, Voc (V) of 0.6, and PCE of 4.3 at Rseries of 73 and Rshunt of 744 for the structure FTO (500 nm)/SnO_2 (70 nm)/$FAPbI_3$ (350 nm)/Spiro-OMeTAD (200 nm)/Au. When we simulated the same structure using the SCAPS tool with the same thickness of the respective layers, the results obtained were Jsc (mA/cm^2) of 15.501581, FF (%) of 25.32, Voc (V) of 1.2137, and PCE of 4.76. The PCE obtained from the simulation is approximately similar. The comparison chart is shown in figure 2.

Table 1. PCs Material Parameters for proposed Structure ITO/ETMs/Absorber/HTMs

Parameters	ITO	ZnO[4]	TiO_2 [5]	IGZO[6]	$FA_{1-x}Cs_xPb(I_{1-x}Br_x)_3$[7]	CBTS[8]	CuO[7]
X (nm)	0.70	0.70	0.70	0.70	01.5	1.00	1.035
E_g, (eV)	3.5	3.3	3.2	3.05	1.59	1.9	1.50
χ (eV)	4	4	4	4.16	4.09	3.6	4.07
ε (Relative)	9	9	10	10	6.6	5.4	18.1
N_c, ($1/cm^3$)	2.2×10^{18}	3.7×10^{18}	1×10^{21}	5.1×10^{18}	2.1×10^{18}	2.2×10^{18}	2.2×10^{19}

N_v (1/cm³)	1.80 x 10^{18}	1.80 x 10^{19}	2 x 10^{20}	5.0 x 10^{18}	2.0 x 10^{18}	1.80 x 10^{18}	5.5 x 10^{20}
V_e (cm/ s)	10^7	10^7	10^7	10^7	10^7	10^7	10^7
V_h (cm/ s^1)	10^7	10^7	10^7	10^7	10^7	10^7	10^7
μ_e (cm^2 /Vs)	20	100	10	15	8.16	30	10^2
μ_h (cm^2/ Vs)	10	25	2 x 10	0.1	2	10	10^{-1}
N_d (1/cm³)	1.0 x 10^{21}	1.0 x 10^{18}	5 x 10^{19}	1. 0 x 10^{17}	1.3 x 10^{16}	0	0
Na (1/cm³)	0	0	0	0	1.3 x 10^{16}	10^{18}	1. 0 x 10^{15}
N_t (1/cm³)	1.0 x 10^{15}	1.0 x 10^{15}	1.0 x 10^{15}	1.0 x 10^{15}	4 × 1013	1.0 x 10^{15}	1.0 x 10^{13}

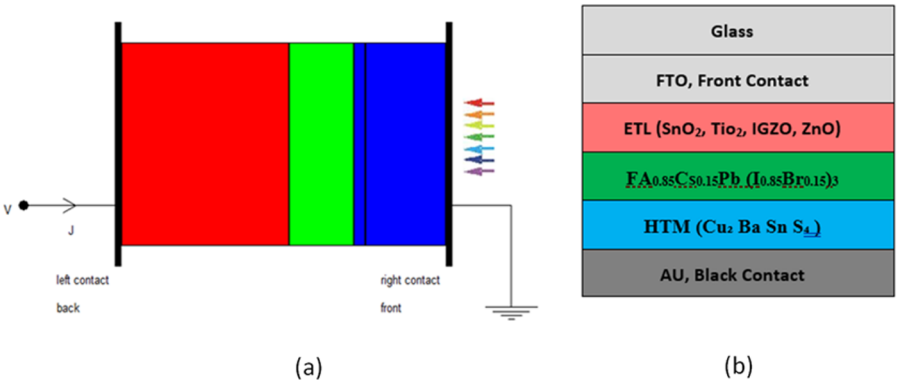

Fig. 1. (a) PSC design (SCAPS-1D) (b) Proposed Layered Schematic of Layers

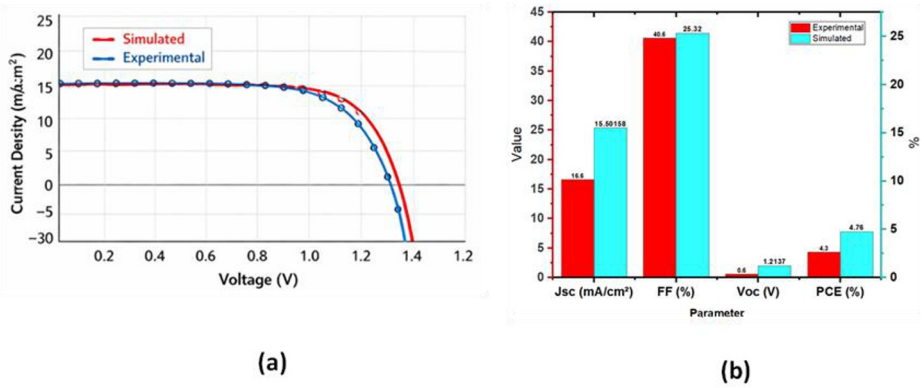

Fig. 2. (a) J-V Characteristic comparison (b) PSC parameters for absorber $FAPbI_3$

Table 2. Interface defect for proposed Structure ITO/ETMs/Absorber/HTMs

Parameters	SnO_2/ $FA_{1-x}Cs_xPb(I_{1-x}Br_x)_3$	ZnO/ $FA_{1-x}Cs_xPb(I_{1-x}Br_x)_3$	IGZO/ $FA_{1-x}Cs_xPb(I_{1-x}Br_x)_3$	Tio2/$FA_{0.85}Cs_{0.15}$ $Pb(I_{0.85}Br_{0.15})_3$
Defect	Neutral	Neutral	Neutral	Neutral
Energy distribution	Single	Single	Single	Single
Capture cross section	$1x10^{-19}$	$1x10^{-19}$	$1x10^{-19}$	$1x10^{-19}$
Energy level	0.6	0.6	0.6	0.6
Total density(1/cm3)	$1x10^{13}$	$1x10^{13}$	$1x10^{13}$	$1x10^{13}$

Table 3. Optimized Performance with Different ETMs in the Proposed Device Structure ITO/ETMs/Absorber/HTMs

ETMs	PCE (%)	Jsc ($mAcm^{-2}$)	Voc (V)	FF (%)
TiO_2	17.10	27.643431	0.7464	82.88
IGZO	16.89	27.395846	0.7463	82.60
SnO_2	16.98	27.549538	0.7458	82.66
ZnO	17.11	27.667216	0.7464	82.87

3 Device Configuration and Simulation Framework

An n–i–p device architecture consisting of FTO/ETL/ $FA_{1-x}Cs_xPb(I_{1-x}Br_x)_3$/ CBTS /Au is employed for the numerical simulations. To model charge carrier generation, the SCAPS simulation (Fig. 1(a)) employs a device configuration illuminated from its right side. A numerical simulation method analyses the performance of one-dimensional structures by solving the governing semiconductor transport and electrostatic equations. Modelling of PSC is based on Poisson's and continuity equations.[9]

Poisson's Equation (Electrostatics)

$$\frac{d}{dx}\left(-\varepsilon(x)\frac{d\psi}{dx}\right) = e[p(x) - n(x) + N_D^+(x) - N_A^-(x) + p_t(x) - n_t(x)] \quad (1)$$

ψ(x) is electrostatic potential, electronic charge (q), n/p is electron/hole concentration, N_D^+ shallow ionized donor density, N_A^- shallow ionized accepter density, pt and nt are trapped holes and electron which is responsible for defect states of perovskite[2]. Gn is electron generation and Rn is recombination rates. Where x is coordinate position, t denotes time, Jn/Jp represents the electrons/holes current density.

Electron Continuity Equation

$$\frac{\partial n(x,t)}{\partial t} = G_n(x,t) + \frac{1}{e}\frac{\partial J_n}{\partial x} - R_n(x,t) \quad (2)$$

$$\frac{\partial p(x,t)}{\partial t} = G_p(x,t) + \frac{1}{e}\frac{\partial J_p}{\partial x} - R_p(x,t) \quad (3)$$

Current Density Equations (Drift–Diffusion Model)

$$J_n = q\mu_n E + qD_n\frac{dn}{dx} \quad (4)$$

$$J_p = q\mu_p E - qD_p\frac{dp}{dx} \quad (5)$$

SRH recombination refers to a non-radiative carrier recombination process in semiconductors.[9]. In this mechanism, charge carriers are captured successively by defect levels, allowing electron–hole recombination to occur without the emission of photons. RRR is an intrinsic recombination process, where an electron transits Ec to unoccupied Ev and recombines with a hole, resulting in the emission of a photon [6,7]. The energy released from this electron-hole annihilation is emitted as electromagnetic radiation, typically as a photon whose energy is close to the bandgap of the material. The rate of radiative recombination can be quantitatively described by a fundamental equation that models this intrinsic process under various conditions. The relationship successfully characterizes the internal physics and accurately predicts simulated behaviour in semiconductor materials.

$$R_{SRH} = \frac{np - n_i^2}{\tau_p(n+n_1) + \tau_n(p+p_1)} \quad (6)$$

$$R_{RR} = B_r(np - n_i^2) \quad (7)$$

$$R_{AR} = (C_n n + C_p p)(np - n_i^2) \quad (8)$$

The terms Cn and Cp coefficients refer specifically to the Auger recombination for electrons and holes. Carrier lifetimes are characterized by τn for electrons and τp for holes. Furthermore, the parameters ni and pi define the electron and hole densities when the defect's trap energy level aligns with the semiconductor's intrinsic Fermi energy.

4 Results and Discussion

4.1 Impact of R_{Series} and S_{hunt} on PSC

In numerical modelling of PSC, the effects of non-ideal electrical behaviour in practical devices are accounted by introducing Rs/Rsh resistance into the simulation framework. A high series resistance leads to reduction in FF (%), and Jsc, Rs is treated as an external lumped resistance connected in series with the device, allowing realistic modelling of resistive transport losses. Figure 2 demonstrates that the device response is strongly influenced by the series resistance present between the front and rear metal contacts, whereas the shunt resistance originates from leakage pathways across the junction. In the analysis, the Rs value spanned 0 to 100 Ω·cm², and the Rsh was adjusted across the interval of 1 kΩ·cm² to 6 kΩ·cm² It is observed that even a slight increase in series resistance (Rs) significantly degrades the device performance. Inefficient charge carrier transport limits effective power extraction from the device. Optical losses during transmission diminish the population of photogenerated charges, which in turn reduces the short-circuit current density (Jsc).With an increase in shunt resistance (Rsh), Voc, fill factor (FF), and PCE show noticeable improvement due to the suppression of leakage currents. The highest efficiency was observed for a configuration with Rs=1 Ω·cm2 and Rsh=104 Ω·cm2, resulting in the following photovoltaic parameters: PCE = 16.27%, FF = 79.19%, Voc = 0.7462 V, and Jsc = 27.54 mA cm^{-2}

4.2 Effect of Temperature on the Proposed PSC

Rising temperature affects charge carrier velocity due to increased phonon scattering, while recombination reduces the effective carrier population, producing an opposite impact on transport. The performance of the proposed device structure is evaluated over a temperature range of 150 K to 400 K, and the corresponding effects on the photovoltaic parameters are systematically analysed. The Voc, FF and PCE decreases significantly with rising temperature because of increased intrinsic carrier concentration and enhanced recombination losses. Fig. 3 shows that increasing temperature marginally improves Jsc due to bandgap narrowing, while Voc and FF decrease from 1.1 to 0.6 V and 84.4% to 78%, respectively, leading to a substantial drop in PCE from 24.5% to 14%. As temperature increases, the open-circuit voltage (Voc) typically decreases due to enhanced intrinsic carrier concentration and increased recombination rates, particularly through Shockley–Read–Hall (SRH) processes. This reduction in Voc leads to a decline in overall power conversion efficiency (PCE). Additionally, higher temperatures can slightly increase short-circuit current density (Jsc) due to improved carrier generation; however, this effect is generally insufficient to compensate for the loss in Voc and fill factor (FF) [16], [17]. Overall, optimal device performance is

typically achieved near room temperature (~300 K), while higher operating temperatures negatively affect both efficiency and long-term stability, making thermal management a critical factor in practical device deployment.

4.3 Effect of Thickness Variation of $FA_{0.85}Cs_{0.15}Pb(I_{0.85}Br_{0.15})$ absorber Layer.

The proposed perovskite solar cell (PSC) utilizes a mixed-cation and mixed-halide perovskite absorber, $FA_{0.85}Cs_{0.15}Pb(I_{0.85}Br_{0.15})$. Partial substitution of iodide (I^-) with bromide (Br^-) allows fine-tuning of the bandgap, improving light absorption in the visible spectrum and optimizing the open-circuit voltage (Voc). The thickness of the absorber layer significantly influences the performance of a perovskite solar cell. Increasing the absorber thickness enhances light absorption within the perovskite layer, which leads to higher generation of electron–hole pairs and an improvement in the short-circuit current density (Jsc). Fig. 3(b) illustrates that increasing the thickness of the absorber layer forces charge carriers to traverse longer distances to reach the electrodes. When the carrier diffusion length is shorter than the layer thickness, many photogenerated carriers recombine before collection, leading to a decrease in the fill factor (FF) and open-circuit voltage (Voc). The optimisation of interfacial defect (fault) density reported in simulation studies is often idealized compared to what can be achieved experimentally. In practical perovskite device fabrication and thin-film solar cells, interface defect densities are typically in the range of 10^{10} to 10^{13} cm^{-2}, depending on the quality of deposition, surface passivation, and interface engineering techniques. In contrast, simulation studies commonly explore a wider range, usually from 10^8 to 10^{16} cm^{-2}, to understand the sensitivity of device performance to recombination losses at the interfaces. Optimized values reported in simulations provide useful theoretical limits and performance trends, Defect densities in the range of 10^{10}–10^{12} cm^{-2} are generally considered practical and achievable in well-fabricated experimental devices. The lower end of this range ($\leq 10^9$ cm^{-2}) represents nearly defect-free or highly passivated interfaces, which are difficult to achieve experimentally but can be approached using advanced techniques such as surface treatments, buffer layers, and defect passivation strategies. The higher range ($\geq 10^{14}$ cm^{-2}) corresponds to poorly fabricated interfaces with significant recombination losses, leading to degraded device performance. For the absorber layer , small thickness variations (±10–20 nm) generally have a limited impact once sufficient thickness is achieved for effective light absorption. thinner layers reduce light absorption and thus decrease Jsc, while excessively thick layers increase recombination losses and series resistance, reducing FF and overall efficiency [16], [17]. For transport layers such as SnO_2 (ETL) and Spiro-OMeTAD (HTL), the device performance is more sensitive to thickness variations. Thin layers may result in incomplete coverage and shunting paths, whereas thicker layers can hinder charge transport and increase resistive losses [18] Additionally, at the interfaces, even slight non-uniformities in thickness can significantly affect band alignment and carrier extraction, particularly in thin-film devices [17], [19]. In practical fabrication techniques like spin coating and vapor deposition, thickness variations of about ±5–10% are common, making precise control essential for achieving consistent device performance. SCAPS-1D assumes uniform bulk mobility and does not explicitly account for microscopic effects such as grain boundaries and

localized trap distributions. Trap-assisted recombination is included in the model through the Shockley–Read–Hall (SRH) recombination mechanism, where defect density, capture cross-sections, and energy levels are defined. the optimized mobility values represent ideal or effective parameters rather than fully realistic transport conditions in experimentally fabricated devices.

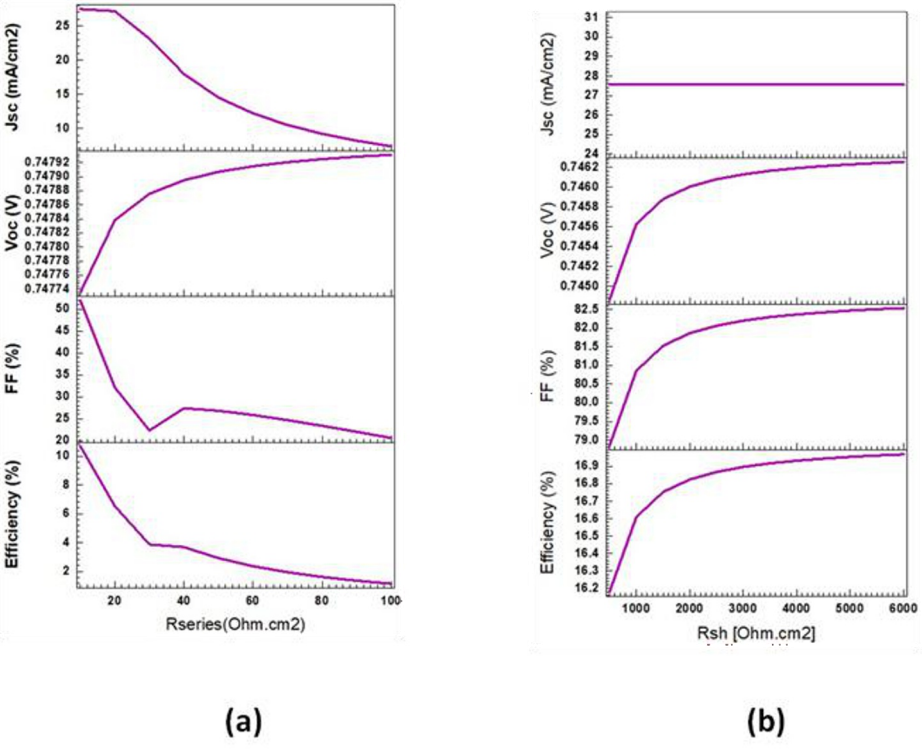

Fig. 3. Effect of series, Shunt on proposed PSC structure ITO/TiO_2/ $FA_{1-x}Cs_xPb(I_{1-x}Br_x)_3$/ Cu_2BaSnS_4 /Au

4.4 Critical Role of HTL/ETL Thickness

Increasing Cu_2BaSnS_4 layer thickness has a pronounced effect on charge transport. 5 depict the impact of varying the Cu_2BaSnS_4 thickness from 5nm to 90 nm on device performance. The enhancement in Jsc and PCE with increasing thickness is primarily attributed to improved hole extraction and suppressed interfacial recombination. The decline in the FF and Voc is mainly associated with increased recombination and resistive losses within the device. In the same way when ETM layer increased ,it is observed all parameter decreases except FF.[10].

4.5 Impact of Varying Perovskite Defect Density (*Nt*)

By systematically varying the defect density (Nt) between 1015 and 1019 1/cm3, Fig. 4 reveals its critical effect on the proposed PSC's operational parameters. The trap states were scanned from the valence band edge up to 1.2 eV into the bandgap, with a baseline established at Et=EV+0.6. The primary origin of defects in the absorber layer is associated with non-uniform dopant incorporation and sub-optimal doping processes in the $FA_{0.85}Cs_{0.15}Pb(I_{0.85}Br_{0.15})$ perovskite. As the defect increases the Jsc reduce from 27.70 to 6.5as it introduces a large number of trap states within the bandgap, which act as strong points for photogenerated charges.[11] In the simulation, the dominant recombination mechanism limiting device performance is typically Shockley–Read–Hall (SRH) recombination, which arises from defect states present in the bulk material and at interfaces. As Nt increases, the density of trap states within the bandgap rises, which enhances Shockley–Read–Hall (SRH) recombination and significantly reduces carrier lifetime. This leads to a decrease in open-circuit voltage (Voc), short-circuit current density (Jsc), and fill factor (FF), ultimately lowering the power conversion efficiency (PCE) of the device. S. De Wolf et al. demonstrated that high-quality perovskite films with low defect densities exhibit longer carrier lifetimes. W. Tress reported that reducing non-radiative recombination through defect passivation significantly enhances open-circuit voltage (Voc) and overall performance.

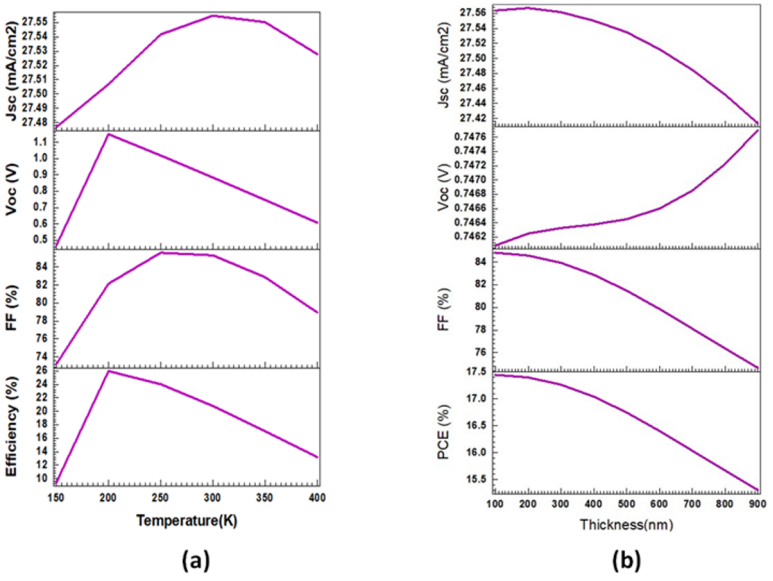

Fig. 4. (a) Effect of Temperature (b) absorber Thickness on proposed PSC structure ITO/TiO_2/ $FA_{0.85}Cs_{0.15}Pb(I_{0.85}Br_{0.15})$/ Cu_2BaSnS_4 /Au

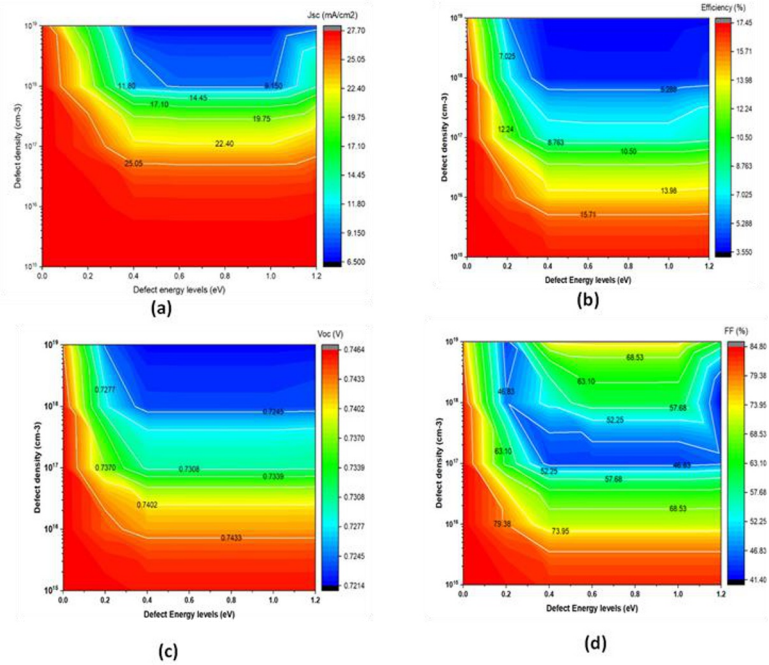

Fig. 5. Contour plots showing the effect of defect density (a)J_{sc} (b)V_{oc} (c) FF (d) PCE

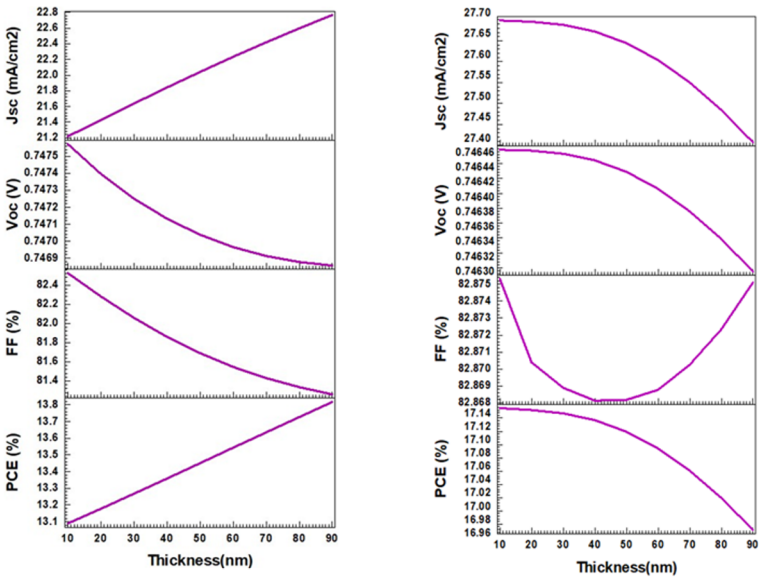

Fig. 6. (a) Effect of Thickness on HTL (b) Effect of ETL on proposed PSC structure ITO/TiO_2/ $FA_{0.85}Cs_{0.15}Pb(I_{0.85}Br_{0.15})$/ Cu_2BaSnS_4 /Au

5 Conclusion

The performance characteristics of the $FA_{0.85}Cs_{0.15}Pb(I_{0.85}Br_{0.15})/Cu_2BaSnS_4$ perovskite solar cell structure are investigated in this study under varying material and electrical parameters.. We investigated the impact of different hole transport layers (HTLs), using Cu_2BaSnS_4 as the HTL, and analyzed the resulting variations in photovoltaic parameters of the PSC. In this study, we examined two planar device architectures: one employing Cu_2BaSnS_4 as the hole transport layer ($ITO/ETL/FA_{0.85}Cs_{0.15}Pb(I_{0.85}Br_{0.15})/Cu_2BaSnS_4/Au$) and the other using CuO ($ITO/ETL/FA_{0.85}Cs_{0.15}Pb(I_{0.85}Br_{0.15})/CuO/Au$), evaluate how the HTL material affects PSC performance. A comparison of the results obtained by numerical simulation is provided in Table 4. The result from [11] is based on costly materials (Spiro-OMeTAD/MXene), an economic disadvantage avoided by using low-cost, earth-abundant Cu_2BaSnS_4.

Table 4 comparison of the results obtained by numerical simulation

Device Structure	Voc(v)	Jsc(mA/cm^2)	FF(%)	PCE	Ref
$ITO/SnO_2/FA/Cu_2BaSnS_4/Au$	1.1366	21.91	81.81	20.37	This Work
$ITO/ZnO/FA/Cu_2BaSnS_4/Au$	1.1369	22.05	81.82	20.52	This Work
ITO/ZnO/FA/CuO/Au	0.7464	27.55	82.87	17.04	This Work
$ITO/SnO_2/FA/CuO/Au$	0.7458	27.54	82.66	16.98	This Work
FTO/SnO2/FA/Spiro OMeTAD/Au/Ti_3C_2Tx	1.28	20.48	67.74	17.85	[11]
FTO/ZnO/FA/Spiro OMeTAD/Au/Ti_3C_2Tx	1.21	22.98	75.37	20.54	[11]

References

1. P. Würfel and U. Würfel, Physics of solar cells : from basic principles to advanced concepts. Wiley-VCH, 2009.
2. K. Deepthi Jayan and V. Sebastian, “Comprehensive device modelling and performance analysis of MASnI3 based perovskite solar cells with diverse ETM, HTM and back metal contacts,” Sol. Energy, vol. 217, no. February, pp. 40–48, 2021, doi: 10.1016/j.solener.2021.01.058.
3. S. Karthick, S. Velumani, and J. Bouclé, “Experimental and SCAPS simulated formamidinium perovskite solar cells : A comparison of device performance,” Sol. Energy, vol. 205, no. March, pp. 349–357, 2020, doi: 10.1016/j.solener.2020.05.041.
4. K. Kumar and P. Giri, “Planar heterojunction formamidinium lead-based perovskite solar cells with MXenes/Au electrode,” Opt. Quantum Electron., vol. 55, no. 8, 2023, doi: 10.1007/s11082-023-05024-z.
5. N. J. Valeti, K. Prakash, and M. K. Singha, “Numerical simulation and optimization of lead free CH3NH3SnI3 perovskite solar cell with CuSbS2 as HTL using SCAPS 1D,” Results Opt., vol. 12, no. April, pp. 1–10, 2023, doi: 10.1016/j.rio.2023.100440.
6. S. Sani, A. Usman, A. Bhatranand, Y. Jiraraksopakun, K. S. Muhammad, and U. Yahaya, “A study on defect, doping, and performance of ETLs (ZnO, TiO2, and IGZO) for the lead-free CsSnCl3 perovskite solar cell by SCAPS-1D framework,” Mater. Today Commun., vol. 38, no. November 2023, 2024, doi: 10.1016/j.mtcomm.2023.107575.
7. I. Qasim, O. Ahmad, and M. Rashid, “(FAPI) -based perovskite solar cell with different ETMs using solar capacitance simulator,” Sol. Energy, vol. 228, no. August, pp. 100–119, 2021, doi: 10.1016/j.solener.2021.09.054.

8. M. K. Hossain et al., "Numerical simulation and optimization of a CsPbI3-based perovskite solar cell to enhance the power conversion efficiency," New J. Chem., vol. 47, no. 10, pp. 4801–4817, 2023, doi: 10.1039/d2nj06206b.
9. R. Pandey, J. Madan, and R. Sharma, "Enhanced Charge Extraction in Metal-Perovskite-Metal Back-Contact Solar Cell Structure through Electrostatic Doping: A Numerical Study," IEEE Trans. Electron Devices, vol. 68, no. 4, pp. 1757–1763, Apr. 2021, doi: 10.1109/TED.2021.3057029.
10. A. K. Singh, S. Srivastava, A. Mahapatra, J. K. Baral, and B. Pradhan, "Performance optimization of lead free-MASnI3 based solar cell with 27% efficiency by numerical simulation," Opt. Mater. (Amst)., vol. 117, Jul. 2021, doi: 10.1016/j.optmat.2021.111193.
11. B. K. Ravidas, M. K. Roy, and D. P. Samajdar, "Investigation of photovoltaic performance of lead-free CsSnI3-based perovskite solar cell with different hole transport layers: First Principle Calculations and SCAPS-1D Analysis," Sol. Energy, vol. 249, no. November 2022, pp. 163–173, 2023, doi: 10.1016/j.solener.2022.11.025.
12. X. Zhang et al., "Controlled synthesis of high efficiency Cu_2BaSnS_4 solar cells via a solution processed method," Materials Letters, vol. 270, 2020.
13. J. Ge and Y. Yan, "Synthesis and characterization of photoelectrochemical and photovoltaic Cu_2BaSnS_4 thin films and solar cells," Journal of Materials Chemistry C, 2017.
14. J. Ge, C. R. Grice, and Y. Yan, "Cu_2BaSnS_4 thin films acting as hole transport layers in perovskite solar cells," Journal of Materials Chemistry A, vol. 5, pp. 2920–2928, 2017.
15. S.Kumar et al., "Cu_2BaSnS_4 quantum dots for photocatalytic applications," Materials Today Communications, 2020.
16. J. Nelson, The Physics of Solar Cells. London, U.K.: Imperial College Press, 2003.
17. S. M. Sze and K. K. Ng, Physics of Semiconductor Devices, 3rd ed. Hoboken, NJ, USA: Wiley, 2007.
18. W. Tress, "Perovskite Solar Cells on the Way to Their Radiative Efficiency Limit," Adv. Energy Mater., vol. 7, no. 14, 2017.
19. N.-G. Park, "Perovskite solar cells: an emerging photovoltaic technology," Mater. Today, vol. 18, no. 2, pp. 65–72, 2015.

Open Access This chapter is licensed under the terms of the Creative Commons Attribution-NonCommercial 4.0 International License (http://creativecommons.org/licenses/by-nc/4.0/), which permits any noncommercial use, sharing, adaptation, distribution and reproduction in any medium or format, as long as you give appropriate credit to the original author(s) and the source, provide a link to the Creative Commons license and indicate if changes were made.

The images or other third party material in this chapter are included in the chapter's Creative Commons license, unless indicated otherwise in a credit line to the material. If material is not included in the chapter's Creative Commons license and your intended use is not permitted by statutory regulation or exceeds the permitted use, you will need to obtain permission directly from the copyright holder.